ACS OMEGA

http://pubs.acs.org/journal/acsodf

Article

Removal of Metal Ions in Phosphoric Acid by Electro-Electrodialysis with Cross-Linked Anion-Exchange Membranes

Xiaoling Duan, Cun-Wen Wang, Tielin Wang, Xiaolin Xie, Xingping Zhou,* and Yunsheng Ye*

Cite This: *ACS Omega* 2021, 6, 32417−32430

Read Online

ACCESS | Metrics & More | Article Recommendations

ABSTRACT: There are numerous metallic impurities in wet phosphoric acid, which causes striking negative effects on industrial phosphoric acid production. In this study, the purification behavior of metallic impurities (Fe, Mg, Ca) from a wet phosphoric acid solution employing the electro-electrodialysis (EED) technology was investigated. The cross-linked polysulfone anion-exchange membranes (AEMs) for EED were prepared using *N*,*N*,*N*′,*N*′-tetramethyl-1,6-hexanediamine (TMHDA) to achieve simultaneous cross-linking and quaternization without any cross-linkers or catalysts. The performance of the resulting membranes can be determined using quaternization reagents. When the molar ratio of trimethylamine/TMHDA/chloromethylated polysulfone is 3:1:1, the cross-linked membrane CQAPSU-3-1 exhibits lower water swelling and membrane area resistance than the non-cross-linked membrane. The low membrane area resistance of CQAPSU-3-1 with long alkyl chains is obtained due to the hydrophilic−hydrophobic microphase separation structure formed by TMHDA. EED experiments with different initial phosphoric acid concentrations of 0.52 and 1.07 M were conducted to evaluate the phosphoric acid purification of different AEMs. The results show that the EED experiments were more suitable for the purification of wet phosphoric acid solution at low concentrations. It was found that the phosphoric acid concentration in the anode compartment could be increased from 0.52 to 1.04 M. Through optimization, with an initial acid concentration of 0.52 M, CQAPSU-3-1 exhibits an enhanced metallic impurity removal ratio of higher than 72.0%, the current efficiency of more than 90%, and energy consumption of 0.48 kWh/kg. Therefore, CQAPSU-3-1 exhibits much higher purification efficiency than other membranes at a low initial phosphoric acid concentration, suggesting its potential in phosphoric acid purification application.

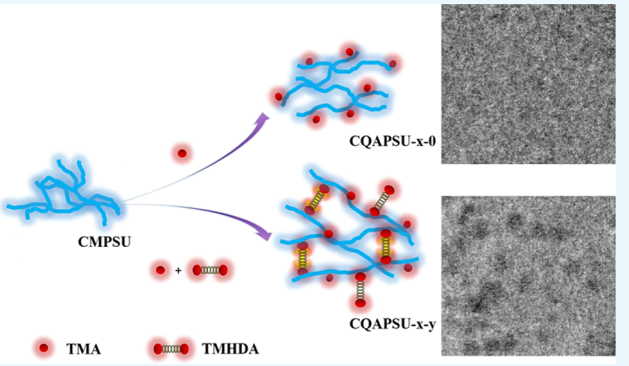

1. INTRODUCTION

There are abundant phosphate rock resources in China but most of them are of mid-and-low grade; the mined mid-and-low grade phosphate rock has aroused considerable interest over the past years. Currently, phosphoric acid produced is manufactured by the wet process and cannot fully meet the industry requirements because of numerous impurities (Fe, Mg, Ca).[1] Several membrane separation techniques, such as reverse osmosis, nanofiltration, and electrodeionization, are used in the wet phosphoric acid purification process for the raw materials.[2,3] Nowadays, among all different types of membrane separation technologies to simply treat wet industrial phosphoric acid, electro-electrodialysis (EED) has received more attention due to its no waste generation and low energy consumption.[4−7] Touaibia et al. selected two perfluorinated anion-exchange membranes (AEMs) in EED experiments for phosphoric acid purification, and the obtained acid possessed a low concentration of metal impurities.[4] Moreover, the heavy metals were removed from the phosphoric acid solution with an EED technique in Ottosen's group.[6]

As a core component of EED, AEM is particularly indispensable to improve ion transport efficiency.[8,9] For EED applications, an ideal AEM must have low enough membrane area resistance to promote the counter-ion transport. The membrane area resistance can be decreased by increasing the functional groups but it causes excessive water swelling.[10] Moreover, the AEM should have good chemical and mechanism stabilities to prolong its working life.[11,12] Hence, the successful preparation of AEMs with high conductivity and stability is one of the most challenging issues for the EED technique.

The comb-shaped structure in AEMs could promote ion transport to achieve high conductivity, and minimize the

Received: July 14, 2021
Accepted: September 17, 2021
Published: November 24, 2021

membrane swelling at the same time.[13,14] We synthesized the comb-shaped polysulfone AEMs with long pendant side chains, which exhibit high ionic conductivity and low water swelling.[15] Wang et al. successfully prepared the ion-nanochannels AEMs, which had the microphase separation structure to enhance the ion transport for waste acid reclamation.[16] Lee et al. synthesized the comb-shaped polysulfone copolymers for fuel cells; the membranes showed higher stability and proton conductivity by hydrophilic−hydrophobic phase separation morphology.[17] Moreover, other researchers also synthesized the comb-shaped AEMs with a lower membrane area resistance and better swelling resistance than the non-comb-shaped AEMs.[13,18−20] Further, the cross-linked network structure in AEMs has been demonstrated as an effective way to enhance the dimensional and mechanical stabilities.[21] Different strategies, such as thiol-ene click chemistry and olefin metathesis were utilized to cross-link AEMs.[22−28] Tibbits et al. prepared the cross-linked hydroxide exchange membranes by a single step via the thiol-ene reaction, which demonstrated reasonable conductivity, better stability, and lower water uptake than other non-cross-linked membranes.[24] Xu et al. synthesized the cross-linked AEMs for electrodialysis by thermal cross-linking of unsaturated moieties and the resultant membranes had high mechanical stability.[29] The challenge in olefin metathesis-based cross-linking methods is the low ion conductivity due to the decreased amount of water absorbed by the formed rigid three-dimensional (3D) networks.[25]

Hence, the high-performance AEMs were prepared by combining the phase separation structure and cross-linking strategy. Xu and co-workers designed the AEMs with long functional side chains and densely cross-linked networks, which possessed excellent tensile strength, dimensional stability, and conductivity.[30] More recently, the synthesis of a cross-linked AEM with commercially available diamines has been proved to be a simple and effective method. The cross-linked AEM was prepared by Shao's group with butyl-substituted doubly charged 1,4-diazabicyclo (2.2.2) octane, which exhibits good flexibility, tensile strength, and a low swelling ratio.[31] Especially, *N*,*N*,*N*′,*N*′-tetramethyl-1,6-hexanediamine (TMHDA) with six methylenes used as a quaternization agent can provide good nano-channels for ion transport and used as a cross-linking agent to improve the mechanical and chemical stabilities.[32−34] Previously, novel double-cross-linked AEMs with good mechanical properties were prepared by Yu and co-workers using TMHDA as a homogeneous quaternization reagent.[35] The cross-linked AEMs were also synthesized with TMHDA in Wu's group, which greatly enhanced the ion selectivity and mechanical properties.[36] However, all of the AEMs were designed and prepared for fuel cells, without considering the possible performance requirements of the EED applications.

In this study, a series of polysulfone AEMs with different amounts of TMHDA and trimethylamine (TMA) were synthesized. The structures of cross-linked AEMs were investigated by Fourier transform infrared (FTIR) spectroscopy, thermogravimetric analysis (TGA), and X-ray photoelectron spectroscopy (XPS) curves. The properties of different AEMs were evaluated systematically using various characterization techniques. Lastly, the EED performances for purifying the phosphoric acid solution were investigated in detail.

2. EXPERIMENTAL SECTION

2.1. Materials. Chloromethylated polysulfone (CMPSU, DCM = 1.23) and wet phosphoric acid solution (C_{H_3PO4} = 0.52 or 1.07 M) were obtained according to our previous work.[10] *N*,*N*,*N*′,*N*′-Tetramethyl-1,6-hexanediamine (TMHDA) was provided by J&K Scientific Ltd. Other chemicals, including *N*,*N*-dimethylformamide (DMF), trimethylamine (TMA), NaOH, $AgNO_3$, NaCl, and KCl were purchased locally. Deionized (DI) water was used in all experiments.

2.2. Membrane Preparation. Dried CMPSU (1 g) was dissolved in DMF (10 mL) at 40 °C. When CMPSU had dissolved completely, different molar ratios of TMA and TMHDA were added to the solution under stirring for 10 min at 25 °C. The obtained solution was degassed and cast on glass plates for 1 h at 25 °C. The solvent was removed by drying at 50 °C for a day and then dried under vacuum at 80 °C to remove the residual solvent completely to get the transparent and flexible cross-linked quaternized ammonium polysulfone membranes (CQAPSU-*x*-*y*, where *x* and *y* represent the molar ratio of TMA and TMHDA to CMPSU, respectively). All membranes were fully converted to the Cl^- form via immersion in 0.5 mol/L NaCl solution for a day, followed by thorough washing with DI water to remove residual ions, and then kept in DI water. Finally, the thickness of the dried membranes was around 60 μm.

2.3. Membrane Characterization. Attenuated total reflectance-Fourier transform infrared spectroscopy (ATR-FTIR) spectra were recorded on a Bruker Equinox 55 spectrometer.

Thermal gravity analysis (TGA) was performed using a Perkin-Elmer TGA-7 instrument with a heating rate of 10 °C/min under the nitrogen atmosphere from 30 to 700 °C.

The X-ray photoelectron spectroscopy (XPS) analysis was obtained on a Shimadzu-Kratos Axis-Ultra DLD-600 W spectrometer using an Al Kα anode.

The surface morphology of the cross-linked membranes was observed with a scanning electron microscope (SEM) in FEI Quanta 200 instrument. The membranes were dried under vacuum and then coated with gold before the measurement.

Transmission electron microscopy (TEM) was performed using a JEOL JEM-2010FEF instrument. The measurements of the membranes morphologies and microstructures were conducted under an accelerating voltage of 200 kV.

Small-angle X-ray scattering (SAXS) was measured on a SAXS LAB ApS system to characterize the membranes' morphologies at room temperature. The correlated parameters were associated with the scattering angle θ.

$$\text{scattering vector} = \frac{4\pi \sin\theta}{0.154} \tag{1}$$

$$\text{Bragg spacing} = \frac{2\pi}{\text{scattering vector}} \tag{2}$$

The cross-linking degree (CD) of cross-linked AEMs can be determined via XPS

$$\text{CD} = \frac{2A_{\text{xQA}}}{2A_{\text{xQA}} + A_{\text{TA}} + A_{\text{QA}}} \tag{3}$$

where A_{xQA}, A_{TA}, and A_{QA} represent the fitting peak area of the cross-linked quaternary ammonium groups, tertiary amine groups, and non-cross-linking quaternary ammonium groups, respectively.

https://doi.org/10.1021/acsomega.1c03720
ACS Omega 2021, 6, 32417−32430

The ion-exchange capacity (IEC) of AEM samples was determined by titrating them with a 0.1 mol/L $AgNO_3$ aqueous solution.[10] The Cl^--form AEMs were dried at 60 °C under vacuum for 24 h and weighed (W_{dry}); then the SO_4^{2-}-form AEMs were obtained after being fully immersed in 0.5 M Na_2SO_4 solution. Subsequently, the experimental IEC values were determined by measuring the consumed volume (V_{AgNO_3}) and concentration (C_{AgNO_3}) of the $AgNO_3$ solution, and the theoretical IEC values were determined by the degree of chloromethylation (DCM) and the molar mass of the cation (M_c).

$$\text{experimental IEC} = \frac{V_{AgNO_3} \times C_{AgNO_3}}{W_{dry}} \times 100\% \quad (4)$$

$$\text{theoretical IEC}_{TMA} = \frac{1000 \times DCM}{442 + DCM \times (M_c - 1)} \quad (5)$$

$$\text{theoretical IEC}_{TMHDA} = \frac{1000 \times DCM}{442 + DCM \times (M_c/2 - 1)} \quad (6)$$

where $M_c = M_a + M_{Cl} + M_{CH_2}$; and M_a, M_{Cl}, and M_{CH_2} are the molar masses of the active groups $N^+(CH_3)_3$ or $(CH_3)_2N^+(CH_2)_6N^+(CH_3)_2$, Cl^-, and $-CH_2$, respectively.

The water uptake (WU) and swelling ratio (SR) were determined by measuring the weight and dimension before and after hydration of AEMs. The weight and dimension of the wet membranes (W_{wet}, L_{length}, L_{width}, L_{thick}) were quickly measured right after removing the excess water on the surface of membranes with filter paper. The weight and dimension of dry membranes (W_{dry}, L'_{length}, L'_{width}, L'_{thick}) were obtained after drying at 60 °C under vacuum for 24 h. After that, the WU, swelling ratio in the plane direction (SR_p) and in the thick direction (SR_t), and the hydration number (λ) were calculated as follows

$$WU = \frac{W_{wet} - W_{dry}}{W_{dry}} \times 100\% \quad (7)$$

$$SR_p = \frac{\sqrt{L_{length} \times L_{width}} - \sqrt{L'_{length} \times L'_{width}}}{\sqrt{L'_{length} \times L'_{width}}} \quad (8)$$

$$SR_t = \frac{L_{thick} - L'_{thick}}{L'_{thick}} \quad (9)$$

$$\lambda = \frac{WU \times 1000}{IEC \times 18 \times 100} \quad (10)$$

The membrane area resistance (R_m) was determined by the alternating current impedance method.[37] The R_m was measured using a two-chamber testing device (effective area: 3.14 cm^2) with 0.5 M NaCl solution in our previous work, which was determined by the entire cell with (R_{m1}) and without (R_{m2}) the membrane.[10]

$$R_m = (R_{m1} - R_{m2}) \times 3.14 \quad (11)$$

The transport number (t^-) was tested using the resistance testing device under a constant current with KCl solution (0.1 M and 0.2 M). The t^- of the anion can be calculated by the potential difference between the electrodes (E_1) and the potential of the standard solution (E_0).

$$t^- = \frac{E_1}{2E_0} \quad (12)$$

where $E_0 = -\frac{RT}{F}\ln\frac{C_2}{C_1}$; C_1 and C_2 are the solution concentration in each compartment; and F, R, and T represent the Faraday constant, gas constant, and temperature, respectively.

The tensile strength (TS) of the hydrated membrane (1 cm × 4 cm) was measured using a CM4104 electric universal tensile machine at a 5 mm/min stretching rate.

For confirming the stability of AEMs at high temperatures and at different concentrations of the phosphoric acid solution, we prepared the phosphoric acid solution at different concentrations (0.5, 1, 2, 3, 5, 10, and 15 M). The IEC values of the CQAPSU-3-0, CQAPSU-3-1, and CQAPSU-3-2 membranes were measured. The AEMs were immersed in each solution at room temperature and in a 15 M phosphoric acid solution at 60 and 80 °C for 24 h. Then, the AEMs were rinsed with DI water.

2.4. Electro-Electrodialysis Experiments for Phosphoric Acid Purification. A series of EED experiments for phosphoric acid purification was performed to evaluate the purification efficiency of the resultant cross-linked AEMs. One cell with two chambers was used by EED at room temperature in our previous works.[10,15] Prior to the test, the AEMs were soaked in 0.52 or 1.07 M phosphoric acid for 24 h and then washed with DI water. After that, the two chambers were separated by one AEM sample, whose effective area was 20 cm^2 (5 cm × 4 cm). The cathode compartment contained 500 mL of the simulated phosphoric acid solution and 500 mL of 0.52 or 1.07 M pure phosphoric acid solution in the anode compartment. During the test, the applied current and the flow rate were kept constant at 0.8 A and 4.5 L/h during all of the experiments. In this experiment, NaOH titration was used to determine the concentration of phosphoric acid in both compartments, and the concentration of metal ions was analyzed by atomic absorption spectrometry.

The current efficiency (η) and energy consumption (E) were obtained from the change in the concentration of phosphoric acid in the anode compartment

$$\eta = \frac{(CV - C_0V_0)F}{It} \times 100\% \quad (13)$$

$$E = \int_0^t \frac{UI\,dt}{(CV - C_0V_0) \times 98} \quad (14)$$

where C and V are the concentration and volume at time t, respectively; C_0 and V_0 are the concentration and volume at time 0, respectively; and U and I are the voltage drop and current across the membrane in the EED.

The removal rates (R_e) of metal ions can be estimated as follows

$$R_e = \frac{C_{mi}^{\,c} - C_{mf}^{\,a}}{C_{mi}^{\,c}} \times 100\% \quad (15)$$

where $C_{mi}^{\,c}$ and $C_{mi}^{\,a}$ are the initial concentrations of metal ions in the cathode compartment and the anode compartment, respectively, and $C_{mf}^{\,a}$ is the final concentration of metal ions in the anode compartment.

https://doi.org/10.1021/acsomega.1c03720
ACS Omega 2021, 6, 32417−32430

Scheme 1. Synthesis Procedure of CQAPSU-*x*-*y*

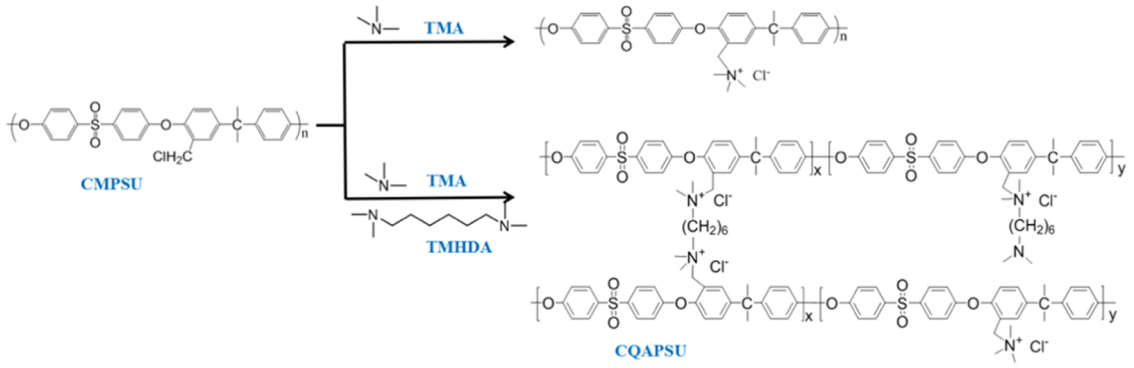

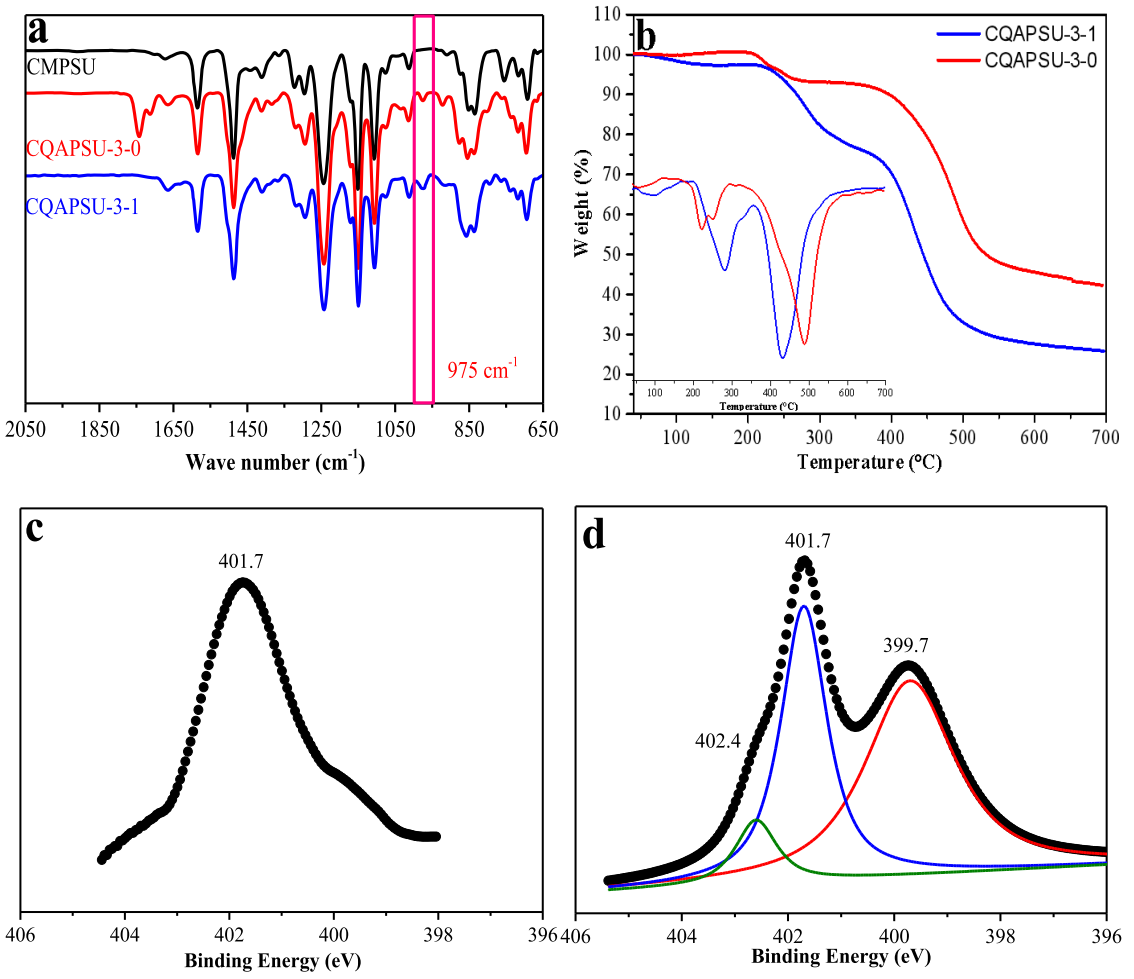

Figure 1. (a) ATR-FTIR spectra of CMPSU, CQAPSU-3-0, and CQAPSU-3-1; (b) TGA and DTG curves of CQAPSU-3-0 and CQAPSU-3-1; and curves of XPS spectra in the N (1s) region of (c) CQAPSU-3-0 and (d) CQAPSU-3-1.

3. RESULTS AND DISCUSSION

3.1. Synthesis and Characterization of AEMs. The synthesis procedure of CQAPSU-*x*-*y* AEMs is shown in Scheme 1 using TMA and TMHDA. TMHDA could easily react with the benzyl chloride groups on CMPSU and acted as both quaternization and cross-linking agents due to its multinitrogen structure.[38] The gelation should be avoided by controlling the quaternary amination reaction time; therefore, excess TMHDA was added to the CMPSU solution for ensuring the complete reaction with chloromethyl groups.[39−41] CQAPSU-*x*-*y* AEMs were fabricated by casting the final reacting solution.

The successful synthesis of CQAPSU-*x*-*y* AEMs was confirmed by ATR-FTIR, XPS, and TGA analysis, as shown in Figure 1. In the case of CQAPSU-3-0 and CQAPSU-3-1, a new peak that appeared at 975 cm^{-1} in Figure 1a shows the presence of C−N stretching, which confirms the quaternary amination of the benzyl chloride groups.

The thermal properties of AEMs depend on the polymer structure and cationic-exchange groups.[32] As seen in Figure 1b, the decomposition behaviors of CQAPSU-3-0 and CQAPSU-

https://doi.org/10.1021/acsomega.1c03720
ACS Omega 2021, 6, 32417−32430

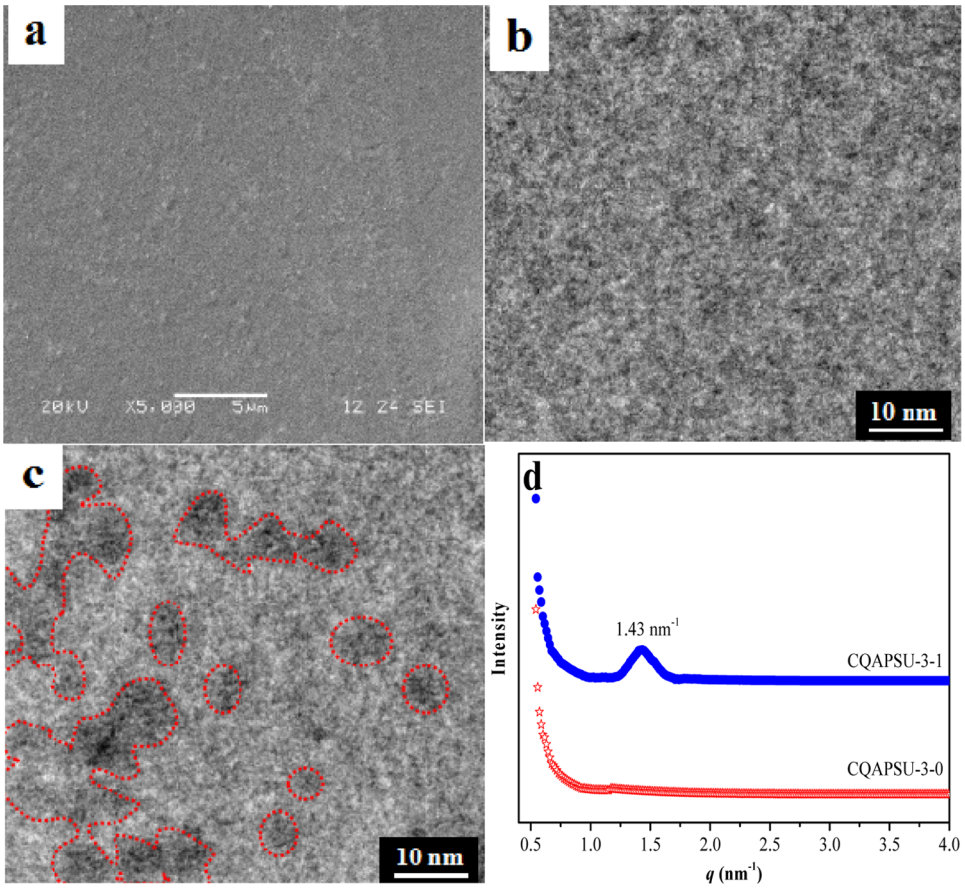

Figure 2. (a) SEM cross-sectional image of CQAPSU-3-1; TEM images of (b) CQAPSU-3-0 and (c) CQAPSU-3-1; and (d) SAXS profiles of CQAPSU-3-0 and CQAPSU-3-1.

3-1 are divided into three stages. The first degradation occurred at around 100 °C and could be attributed to the weight loss of the residual solvent and water evaporation: in the second stage (200−350 °C), the degradation of the ammonium functional groups occurs, and in the third stage, around 360 °C, degradation of the polymer backbones occurs.[42,43] As mentioned above, the thermal stability of CQAPSU-*x*-*y* below 100 °C could meet the requirements of the membrane preparation and EED application.

Figure 1c,d shows the XPS analysis of CQAPSU-3-0 and CQAPSU-3-1 to identify the presence of three different types of functional groups (quaternary ammonium group, tertiary amine group, and cross-linked quaternary ammonium group). There is only one peak at 401.7 eV, corresponding to N (1s) appearing in the XPS spectrum of CQAPSU-3-0 in Figure 1c, which could be attributed to the quaternary ammonium groups without any cross-linking. Figure 1c,d exhibits three different kinds of N (1s) in CQAPSU-3-1: tertiary amine groups at 399.7 eV, cross-linked quaternary ammonium groups at 402.4 eV, and a peak at 401.7 eV corresponding to N (1s) appearing in the XPS spectrum of quaternary ammonium groups like CQAPSU-3-0, respectively.[44] It was confirmed by FTIR, TGA, and XPS spectra that the CQAPSU-*x*-*y* AEMs were successfully synthesized.

3.2. Microstructure and Morphology of AEMs. The ion migration of AEMs is influenced by the microphase morphology of the membranes.[45−47] The long hydrophobic side chain facilitates the aggregation of ion clusters and the formation of ionic domains.[48] The CQAPSU-*x*-*y* with six methylene side chains may exhibit a good microphase separation structure. The morphologies of CQAPSU-3-0 and CQAPSU-3-1 were examined by SEM, TEM, and SAXS analysis as shown in Figure 2.

The SEM image of CQAPSU-3-1 in Figure 2a shows a dense and homogeneous cross-sectional morphology without any holes. Generally, the dark region in TEM images usually represents the hydrophilic ion channels, and the light region denotes the hydrophobic domains. There is no obvious hydrophilic−hydrophobic phase separation structure in CQAPSU-3-0 (Figure 2b). However, the CQAPSU-3-1 exhibits the microphase separation structure as shown in Figure 2c. This is because the structure of the long side chain provides a good phase separation with large ionic domains. The better the microphase separation and larger ion clusters size, and the lower the membrane resistance and faster ion migration.[49] In addition, there is no obvious scattering peak for CQAPSU-3-0 in Figure 2d, indicating no characteristic phase separation for CQAPSU-3-0; whereas, the CQAPSU-3-1 with a long alkyl side chain shows a scattering peak at 1.43 nm^{-1}, suggesting that better interconnected ion channels are formed. Furthermore, the dimension of the characteristic peak of the corresponding ion clusters is 4.4 nm, which agrees well with the TEM observation. It is noteworthy that the effect of cross-linking on the microphase separation structure of CQAPSU-*x*-*y* is small.[50,51]

3.3. Characterization of Physicochemical Properties of AEMs. *3.3.1. IEC and CD of AEMs.* The IEC and CD are the two significant parameters that influence the properties of

https://doi.org/10.1021/acsomega.1c03720
ACS Omega 2021, 6, 32417−32430

Table 1. Effects of the Quaternary Amination Reagent Versus IEC and CD of CQAPSU-*x*-*y*

AEMs	n_{CMPSU} (mmol)	n_{TMA} (mmol)	n_{TMHDA} (mmol)	IEC_T[a] (mmol/g)	IEC_E[b] (mmol/g)	CD[c] (%)
CQAPSU-1-1	1	1	1	2.11	1.57	53.4
CQAPSU-2-1	1	2	1	2.11	1.74	51.5
CQAPSU-3-1	1	3	1	2.11	1.88	49.6
CQAPSU-3-2	1	3	2	2.11	1.82	50.8
CQAPSU-3-3	1	3	3	2.11	1.78	51.7
CQAPSU-3-0	1	3	0	2.14	1.90	

[a]Theoretical IEC. [b]Experimental IEC. [c]Cross-linking degree of the membranes.

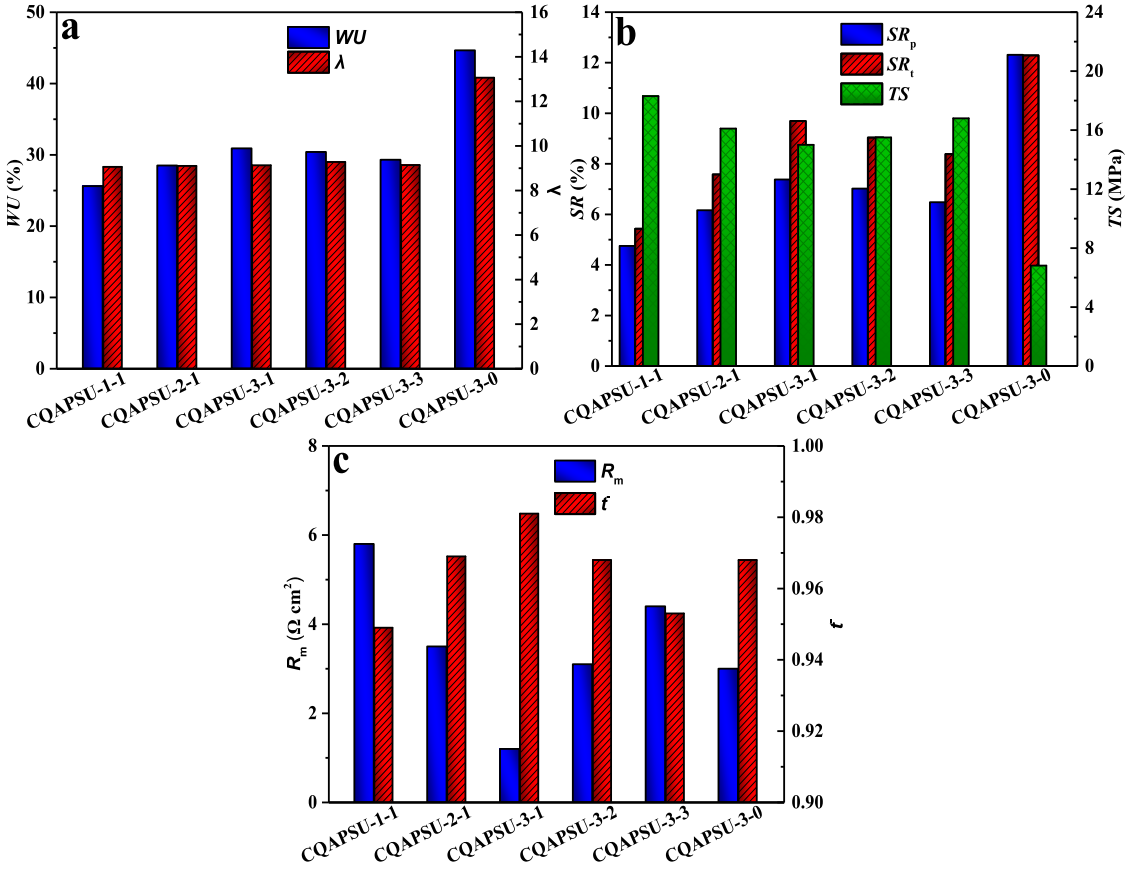

Figure 3. (a) WU and λ; (b) the SR in the plane and thick direction, and the TS; and (c) R_m and t^- of CQAPSU-*x*-*y* at room temperature.

the cross-linked AEM in the EED process and they play a crucial role in terms of conductivity, selectivity, and mechanical strength, which can be determined by the amount of the quaternary amination reagent.[11,52,53] As shown in Table 1, six different AEMs with varying molar ratios of TMA and TMHDA were synthesized. The membrane from CQAPSU-3-0 was functionalized with only TMA, whereas the membranes from CQAPSU-1-1 to CQAPSU-3-3 were prepared using both TMA and TMHDA by the quaternary amination reaction.

A higher IEC resulted in higher ion transport and membrane selectivity.[32] Table 1 shows the IEC values of CQAPSU-*x*-*y* with different amine/polymer ratios. The IEC values increased from CQAPSU-1-1 to CQAPSU-3-1 with an increase in the amount of TMA because the chloromethyl groups on the main chain could be more easily replaced to form sufficient anion exchange sites, and a larger number of quaternary ammonium groups were incorporated into the membrane. Moreover, by increasing the TMHDA amount, the IEC values decreased from CQAPSU-3-1 to CQAPSU-3-3 and can be attributed to the molecular weight of TMHDA being greater than that of TMA. The bulky molecules of TMHDA will result in more steric hindrance in the membrane than that of TMA.[8] The IEC value of CQAPSU-3-1 is closer to that of CQAPSU-3-0 under the same DCM, which indicates that the cross-linked structure of CQAPSU-*x*-*y* does not reduce the IEC values by the functional groups.[20] Furthermore, the experimental IEC values are quite close to the theoretical IEC values, which suggested that all of the chloromethyl groups are converted to ammonium groups.

The CD of CQAPSU-*x*-*y* calculated from the XPS spectrum decreased from 53.4 to 49.6% with the increase of TMA and increased from 49.6 to 51.7% by an increase of TMHDA. Abundant of TMA grafted to the polymer will reduce the cross-linking between TMHDA and chloromethyl groups. The grafting degree of the tertiary amine groups increased with the increase of TMHDA; however, quaternization of chloromethyl groups was not 100% due to the limited exchange capacity of TMHDA, which implied that the residual chloromethyl groups can be reacted with the tertiary amine groups and obtained a

https://doi.org/10.1021/acsomega.1c03720
ACS Omega 2021, 6, 32417−32430

higher CD.[54,55] As presented in Table 1, CQAPSU-3-1 has the highest IEC value and lowest CD, except CQAPSU-3-0, which has a large steric resistance due to TMHDA with long alkyl chains.

3.3.2. WU, λ, SR, TS, R_m, and t^- of AEMs. Generally, the physicochemical and electrochemical properties such as water swelling and ion transport of non-cross-linked AEMs are determined by the IEC values. The higher IEC values increase the area of hydrophilic domains and water swelling of non-cross-linked AEM.[53] However, it was found that the related properties of cross-linked AEMs are dependent not only on IEC values but also on the CD.[11]

As shown in Figure 3a,b, the WU and SR of CQAPSU-*x*-*y* increased by increasing TMA and decreased as TMHDA increased. The higher IEC values correspond to the lower CD as shown in Table 1; the TMA effectively reduced the interaction between adjacent polymers and promoted the water molecules into AEMs.[9] Therefore, the WU and SR of CQAPSU-*x*-*y* increased as CD decreased. CQAPSU-3-1 exhibits the highest WU and SR. Subsequently, the WU and SR of CQAPSU-*x*-*y* decreased as CD and TMHDA increased by impeding the water molecules into the membranes. The SR_p values of CQAPSU-*x*-*y* are all lower than SR_t in Figure 3b, which suggests that the cross-linked network structure enhanced the membrane swelling resistance in the plane but not enhanced in the thick direction.[33] λ, the number of water molecules per ion, was determined by the polymer structure and WU. Figure 3a shows that the λ remains invariant with the increase of TMA and TMHDA, and it is believed that the water adsorption capacity has not been improved with the cross-linked structure of CQAPSU-*x*-*y*. The WU of CQAPSU-3-1 (30.9%) was lower than CQAPSU-3-0 (44.7%) at a similar IEC value because the cross-linked network of the AEM will adsorb fewer water molecules. The CQAPSU-*x*-*y* possesses good swelling resistance and connected ion-conducting channels by cross-linking and microphase separation structures, respectively. All of the results indicated that the prepared CQAPSU-*x*-*y* with a strong cross-linked network structure has remarkable dimensional stability, which can run in the EED process for a long time.

As reported, the cross-linked AEMs have great mechanical strength in EED application because of the rigid and compact cross-linked structure.[8] The TS of CQAPSU-*x*-*y* in the fully hydrated state was measured at room temperature. As shown in Figure 3b, the TS slightly decreased and improved with increasing the amount of TMA and TMHDA for CQAPSU-*x*-*y*, respectively. It is found that the TS values are in the range of 18.3−15.0 MPa, which are higher than that of the non-cross-linked CQAPSU-3-0 (6.8 MPa). The TS increased with the increase of CD, which limits the movement of polymer chains by the cross-linked network. Accordingly, the excellent mechanical strengths of CQAPSU-*x*-*y* AEMs are efficient for EED application.

The high conductivity and selectivity are the critical performance metrics for AEMs, which is indicative of efficiency for a realistic EED operation.[56−58] Generally, the cross-linked structure is beneficial to enhance the swelling resistance but reduces the conductivity of AEMs.[9] However, the prepared CQAPSU-*x*-*y* membranes show low R_m (in Figure 3c), despite the low WU and SR. It is an increasing trend with the increasing TMHDA content and with decreasing TMA content, respectively. Moreover, the t^- values of CQAPSU-*x*-*y* are in the range of 0.90−0.98. The CQAPSU-*x*-*y* with long alkyl side chains exhibits a good microphase separation structure, which facilitates the ionic clusters formed and ionic conduction.[48] It is believed that increasing the quaternary ammonium groups commonly results in the suppression of co-ions diffusion and improvement of counter-ions passing through the AEM.[11,59,60] The R_m and t^- of CQAPSU-*x*-*y* are found to decrease from 5.8 to 1.2 Ω cm^2 and increase from 0.95 to 0.98 with enhancing charge density by the addition of more TMA or more quaternary ammonium groups, respectively. A good microphase separation structure in AEM will promote the dissociation of charged functional groups and the transportation of ions. CQAPSU-3-1 exhibits the lowest R_m and highest t^-, which indicates that the cross-linked membrane can satisfy the basic requirements of EED application.

Figure 4 represents the stability of AEMs under acidic conditions at room temperature, 60, and 80 °C for 24 h. After

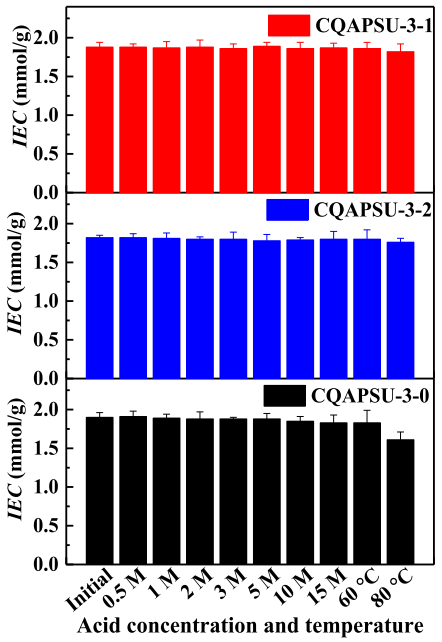

Figure 4. Acid stability at room temperature and stability in 15.0 M phosphoric acid solution at 60 and 80 °C of CQAPSU-*x*-*y*.

CQAPSU-3-0, CQAPSU-3-1, and CQAPSU-3-2 were immersed in phosphoric acid solution at concentrations between 0.5 and 15.0 M, their IEC values did not vary greatly from the initial values obtained prior to immersion. In addition, CQAPSU-3-0, CQAPSU-3-1, and CQAPSU-3-2 exhibited similar IEC values before and after they were stored in 15.0 M phosphoric acid solution at 60 °C, while the IEC values of CQAPSU-3-1 and CQAPSU-3-2 stored in 15.0 M phosphoric acid solution at 80 °C slightly decreased from the values obtained prior to immersion; the IECs of CQAPSU-3-0 stored in 15.0 M phosphoric acid solution at 80 °C decreased from 1.90 to 1.61 mmol/g. As a result, we conclude that the CQAPSU-3-0, CQAPSU-3-1, and CQAPSU-3-2 exhibited acid stability in the phosphoric acid concentration range between 0.5 M and 15.0 M. In addition, CQAPSU-3-0, CQAPSU-3-1,, and CQAPSU-3-2 were stable in 15.0 M phosphoric acid solution at 60 °C, while the cross-linked membrane CQAPSU-3-1 and CQAPSU-3-2 exhibited stability in 15.0 M phosphoric acid solution at 80 °C. The working temperature and acid concentration for the AEMs for EED application are below 60

https://doi.org/10.1021/acsomega.1c03720
ACS Omega 2021, 6, 32417−32430

Table 2. Physicochemical Properties of CQAPSU-*x*-*y*

AEMs	IEC (mmol/g)	CD (%)	WU (%)	SR_p (%)	R_m (Ω cm^2)	t^-	TS (MPa)
CQAPSU-3-1	1.88	49.6	30.9	7.4	1.2	0.98	15.0
CQAPSU-3-2	1.82	50.8	30.4	7.0	3.1	0.97	15.5
CQAPSU-3-0	1.90		44.7	12.3	3.0	0.97	6.8

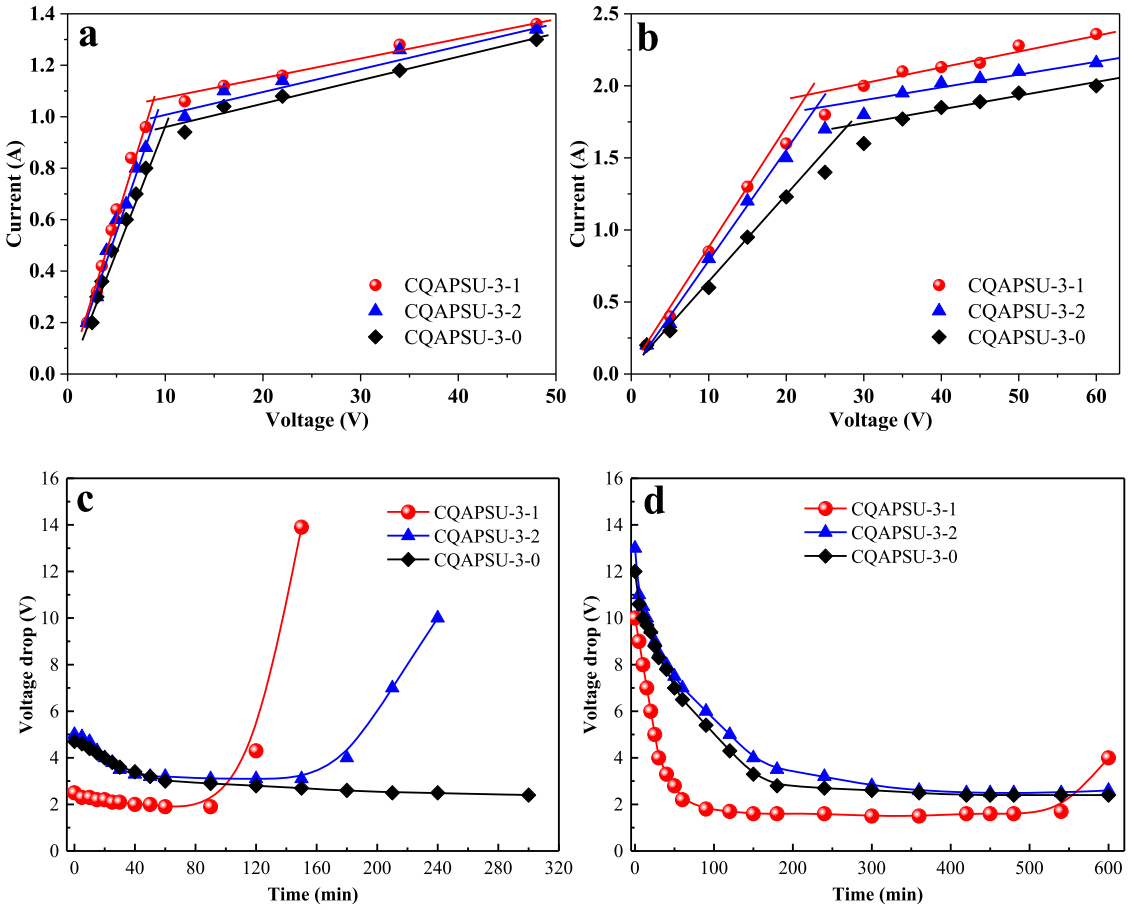

Figure 5. Plots of the current versus voltage at an initial phosphoric acid concentration of (a) 0.52 M and (b) 1.07 M, and the voltage drop at an initial phosphoric acid concentration of (c) 0.52 M and (d) 1.07 M versus operation time for CQAPSU-*x*-*y*.

°C and 10 M. All of the results indicated that the prepared CQAPSU-*x*-*y* membranes with a strong cross-linked network structure have remarkable acid and thermal stability, which can run in the EED process for a long time.

Above all, the addition of TMHDA effectively modified the membrane ion transport and dimensional stability by the microphase separation structure and the cross-linked network structure. The effects of the molar ratio of TMA, TMHDA, and CMPSU were found to influence the IEC and membrane area resistance of the CQAPSU-*x*-*y* AEMs such that the molar ratio should be controlled. The ideal molar ratio of TMA, TMHDA, and CMPSU was determined here to be 3:1:1.

3.4. EED for Phosphoric Acid Purification. The cross-linked membranes CQAPSU-3-1, CQAPSU-3-2, and the non-cross-linked membrane CQAPSU-3-0 were used in a laboratory-scale EED experiment of phosphoric acid purification at room temperature. The physicochemical properties of three AEMs are given in Table 2. We can see from Table 2 that CQAPSU-3-1 and CQAPSU-3-0 show similar IEC values but different water swelling and membrane selectivities. Furthermore, CQAPSU-3-2 and CQAPSU-3-0 show different water swelling and mechanical stabilities under similar membrane selectivity. The initial phosphoric acid concentration is the key factor that can affect the EED performance.[61] Therefore, the initial phosphoric acid concentrations of 0.52 and 1.07 M were investigated, respectively.

Voltage drop is one of the most important parameters affecting the energy consumption of the EED experiment and the working life of AEM.[62,63] As shown in Figure 5a, the limiting currents of AEMs were 0.9−1.1 A at an initial phosphoric acid concentration of 0.52 M, and the high current uses less operation time when other parameters were kept constant.[15] Also, the limiting currents of AEMs were higher than 1.6 A at an initial phosphoric acid concentration of 1.07 M in Figure 5b; for comparison, a current of 0.8 A was used in our experiment. Figure 5c,d shows that the trend of voltage drop curves at different initial phosphoric acid concentrations for different AEMs was similar. With water diffusion and ions transport, the whole membrane stack resistance decreased so that the voltage drop decreased accordingly at the beginning of the experiment. Then, the voltage drop of CQAPSU-3-0 was stable when the conductivity of the solution in the anode and cathode compartments was at high levels (Figure 5c), which suggests that the resistance of the whole stack remains almost

https://doi.org/10.1021/acsomega.1c03720
ACS Omega 2021, 6, 32417−32430

constant;[64] whereas the voltage drop of CQAPSU-3-1 and CQAPSU-3-2 increased dramatically after 100 and 180 min at an initial phosphoric acid concentration of 0.52 M (Figure 5c). These results can be attributed to the fact that the current density is higher than the limit current density and the proton leakage is reduced by the densely cross-linked network structure. As mentioned above, all of the $H_2PO_4^-$ ions were transported from the cathode compartment to the anode compartment in a shorter period of time, and then the experiment was complete. Therefore, the operation time of CQAPSU-3-1 is shortened at a low initial phosphoric acid concentration. When the initial phosphoric acid concentration increased to 1.07 M at constant current, the voltage drop was higher at the starting point of the operation due to the high electrical resistance of the phosphoric acid solution and then decreased sharply by the first stage dissociation of phosphoric acid accelerating (Figure 5d).[10] The voltage drop of CQAPSU-3-1 increased statistically until after 550 min at a high initial phosphoric acid concentration, and the other two AEMs remained stable. This can be ascribed to the change in the electrical resistance of the phosphoric acid solution and membrane resistance. As depicted in Figure 5, the lower the membrane area resistance, the smaller the voltage drop. That is, CQAPSU-3-1 exhibits the lowest voltage drop, which is caused by the minimum membrane area resistance of 1.2 Ω cm^2. In addition (compare Figure 5c,5d), the higher the initial phosphoric acid concentration, the longer the time required for the experiment. This may be due to the fact that when the phosphoric acid concentration is 1.07 M, the $H_2PO_4^-$ ions take longer to transport from the cathode compartment to the anode compartment. In addition, the voltage drop at a high phosphoric acid concentration (Figure 5d) was slightly less than the low concentration (Figure 5c), just at the later stage of the experiment. This was because of the lower resistance of the whole stack.

Figure 6 shows the results of treating AEMs at different concentrations of phosphoric acid. The phosphoric acid concentration increased gradually in the anode compartment, whereas it decreased in the cathode compartment with time elapse for all AEMs, indicating the continuous transport of $H_2PO_4^-$ ions from the cathode compartment to the anode compartment. Meanwhile, CQAPSU-3-1 and CQAPSU-3-2 show higher phosphoric acid concentrations in the anode compartment than that of CQAPSU-3-0 and vice versa. This is due to the cross-linked membranes with long alkyl side chains formed a good microphase separation structure for promoting $H_2PO_4^-$ ions transport.[45] It can be seen that in Figure 6a the phosphoric acid concentration of CQAPSU-3-1 and CQAPSU-3-2 reduced to 0 in the cathode compartment and reached a maximum in the anode compartment at 150 and 240 min, respectively. The CQAPSU-3-2 required more experimental time due to its higher membrane area resistance than CQAPSU-3-1. In addition, CQAPSU-3-0 shows a lower counterion migration rate and the EED experiment needs at least 360 min because of the high membrane area resistance.[64] The phosphoric acid concentration increased more rapidly at the beginning, which is due to less proton leakage. The greater the initial phosphoric acid concentration, the longer the operation time needed due to the more phosphoric acid required to be transported (Figure 6). Moreover, the phosphoric acid concentration of CQAPSU-3-1 takes at least 600 min to reach the maximum in the anode compartment and was reduced to 0 in the cathode compartment an initial

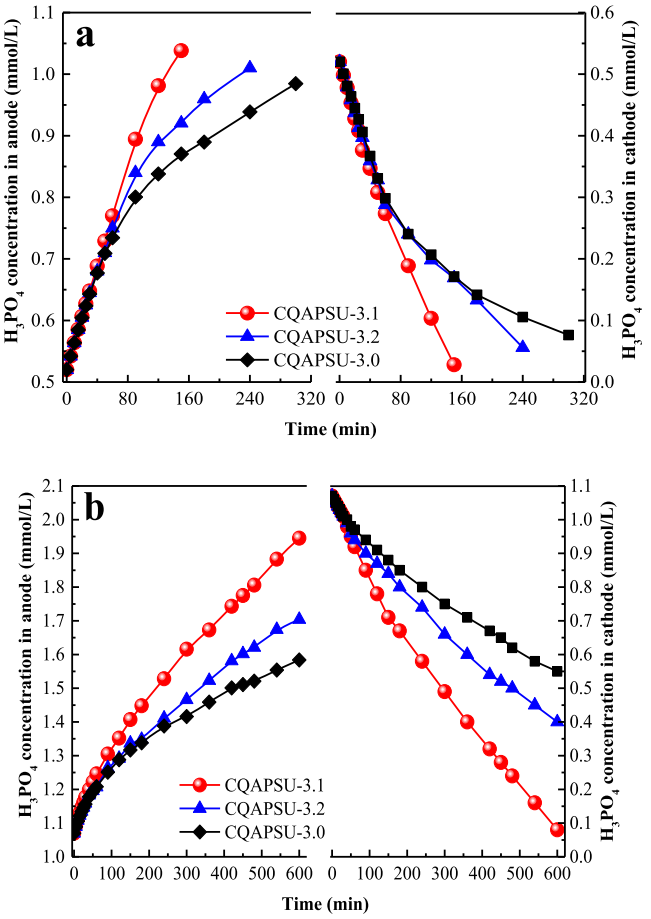

Figure 6. Plots of phosphoric acid concentration at an initial phosphoric acid concentration of (a) 0.52 M and (b) 1.07 M versus operation time for CQAPSU-*x*-*y*.

phosphoric acid concentration of 1.07 M, as shown in Figure 6b, which is 4 times as much as the initial phosphoric acid concentration of 0.52 M. This may be due to the high phosphoric acid concentration resulting in a more amount of $H_2PO_4^-$ needed to be transported from the cathode compartment to the anode compartment. We can see from Figure 6 that the phosphoric acid concentration in the anode compartment with CQPASU-3-1 could be increased from 0.52 M to 1.04 M, and from 1.07 to 1.95 M, respectively. However, it is found that the effective concentration of CQAPSU-3-2 and CQAPSU-3-0 was not very good, as shown in Figure 6b. As a consequence, the cross-linked AEM can be successfully applied for the phosphoric acid concentration at a relatively low initial phosphoric acid concentration.

As shown in Figure 7, the current efficiency decreased with time due to proton leakage.[65] Therefore, CQAPSU-3-1 and CQAPSU-3-2 show much higher current efficiency than CQAPSU-3-0, which can be attributed to the great phase separation structure and low proton leakage rate. Before 100 min, the current efficiency of CQAPSU-3-1 was higher than 90% (Figure 7a) because of the low proton leakage and subsequently decreased with the increasing voltage drop. The current efficiency was decreased slowly for the first 100 min and then decreased faster at a low initial phosphoric acid concentration (Figure 7a). However, the current efficiency sharply decreased at a high initial phosphoric acid concentration (Figure 7b). In addition, the greater the initial

https://doi.org/10.1021/acsomega.1c03720
ACS Omega 2021, 6, 32417−32430

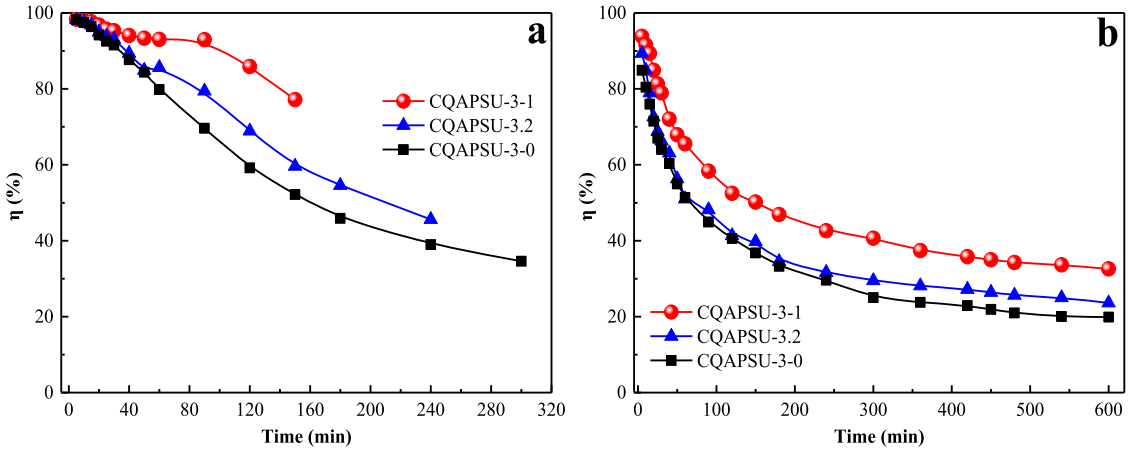

Figure 7. Plots of current efficiency at an initial phosphoric acid concentration of (a) 0.52 M and (b) 1.07 M versus operation time for CQAPSU-*x*-*y*.

phosphoric acid concentration, the lower the current efficiency. It is easy to understand that because a high phosphoric acid concentration resulted in a longer transport time and lower membrane selectivity, more co-ions will migrate through the AEM, which leads to a reduction in the loss of the current efficiency.[61] These results indicate that the CQAPSU-3-1 membrane at a low initial phosphoric acid concentration of 0.52 M shows the highest and the most stable current efficiency in EED.

The final phosphoric acid purification effect and energy consumption of CQAPSU-3-1, CQAPSU-3-2, and CQAPSU-3-0 are shown in Figure 8. As depicted in Figure 8a, the purification rates of CQAPSU-3-1 and CQAPSU-3-2 are higher than 72 wt %. The structure compactness of the membrane increased with the increase of the cross-linking degree, which will restrain the metal ions migration through the AEM.[59,60] Figure 8b shows that the removal rate of metal ions decreases with the increase of the initial phosphoric acid concentration, which is due to the co-ions transport being promoted by the increasing electrolyte concentration. It is worth noting that CQAPSU-3-2 exhibits a slightly higher purification rate than that of CQAPSU-3-1 due to the higher cross-linking degree of the cross-linked AEM. Figure 8 also shows the energy consumption of different AEMs. The energy consumption of CQAPSU-3-1 (0.48 kWh/kg) is far below CQAPSU-3-0 (1.25 kWh/kg) and CQAPSU-3-2 (1.30 kWh/kg) due to the low membrane area resistance and short operation time. It can be found that the energy consumption increased with the increasing initial phosphoric acid concentration, which is in good agreement with the back diffusion of all ions and water transfer at higher concentrations.[66] The low-energy consumption may be beneficial to prolong the AEM lifetime.

According to the above results, it is evident that CQAPSU-*x*-*y* AEMs, especially the CQAPSU-3-1, possess long side chains that showed good dimensional stability (with a cross-linked network structure) and excellent conductivity (with a microphase separation structure), which lead to great concentration and purification effect of phosphoric acid at a low initial phosphoric acid concentration.

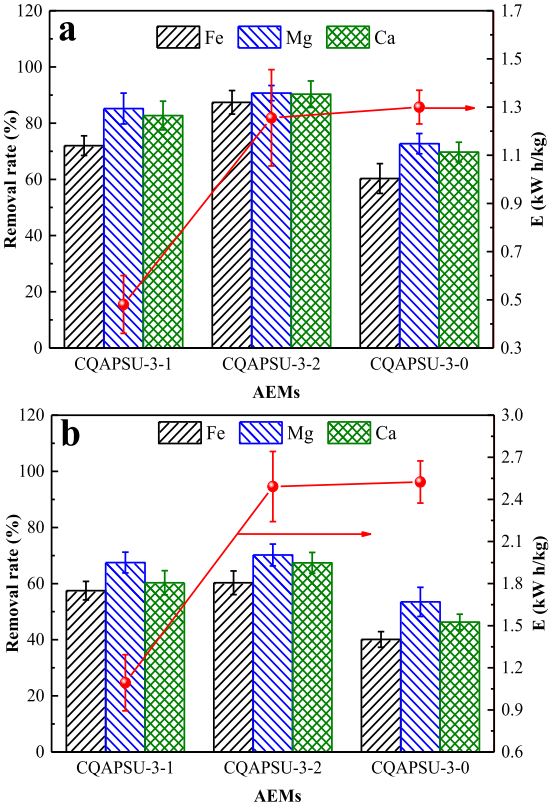

Figure 8. Plots of removal rate of metal ions and energy consumption at an initial phosphoric acid concentration of (a) 0.52 M and (b) 1.07 M versus operation time for CQAPSU-*x*-*y*.

4. CONCLUSIONS

In this study, the cross-linked polysulfone AEMs were successfully synthesized using TMHDA and TMA as cross-linking and quaternization reagents. The cross-linked membranes have great swelling resistance and mechanical properties and high conductivity at room temperature. Especially, CQAPSU-3-1 exhibits the lowest membrane area resistance of 1.2 Ω·cm^2 and appropriate mechanical strength of 15.0 MPa. The excellent performances of cross-linked AEMs are obtained by the cross-linked network structure and the microphase separation structure.

A wet phosphoric acid solution containing metallic impurities (Fe, Mg, Ca) is separated by the EED technique. Compared with non-cross-linked membrane CQAPSU-3-0, the cross-linked membrane CQAPSU-3-1 exhibits the best

https://doi.org/10.1021/acsomega.1c03720
ACS Omega 2021, 6, 32417−32430

concentration effect from 0.52 to 1.04 M, a shortest operation time of 150 min, the highest metal ion removal rate of more than 72.0%, the greatest current efficiency of more than 90%, and energy consumption of 0.48 kWh/kg at an initial phosphoric acid concentration of 0.52 M. It is believed that the optimized CQAPSU-3-1 can be used in the EED experiment for phosphoric acid purification at a low initial phosphoric acid concentration.

AUTHOR INFORMATION

Corresponding Authors

Xingping Zhou − *Key Laboratory of Material Chemistry for Energy Conversion and Storage, Ministry of Education, School of Chemistry and Chemical Engineering, Huazhong University of Science and Technology, Wuhan 430074, China;* orcid.org/0000-0001-9886-7961; Email: xpzhou@mail.hust.edu.cn

Yunsheng Ye − *Key Laboratory of Material Chemistry for Energy Conversion and Storage, Ministry of Education, School of Chemistry and Chemical Engineering, Huazhong University of Science and Technology, Wuhan 430074, China;* orcid.org/0000-0002-2351-1845; Email: ysye@hust.edu.cn

Authors

Xiaoling Duan − *Hubei Key Laboratory of Purification and Application of Plant Anti-Cancer Active Ingredients, School of Chemistry and Life Sciences, Hubei University of Education, Wuhan 430205, China; Key Laboratory of Material Chemistry for Energy Conversion and Storage, Ministry of Education, School of Chemistry and Chemical Engineering, Huazhong University of Science and Technology, Wuhan 430074, China*

Cun-Wen Wang − *Key Laboratory for Green Chemical Process of Ministry of Education, Wuhan Institute of Technology, Wuhan 430073, China*

Tielin Wang − *Key Laboratory for Green Chemical Process of Ministry of Education, Wuhan Institute of Technology, Wuhan 430073, China*

Xiaolin Xie − *Key Laboratory of Material Chemistry for Energy Conversion and Storage, Ministry of Education, School of Chemistry and Chemical Engineering, Huazhong University of Science and Technology, Wuhan 430074, China;* orcid.org/0000-0001-5097-7416

Complete contact information is available at: https://pubs.acs.org/10.1021/acsomega.1c03720

Notes

The authors declare no competing financial interest.

ACKNOWLEDGMENTS

The work was supported by the Science and Technology Research Project of the Education Department of Hubei Province, China (No. B2020177) and the National Natural Science Foundation of China (52020105012). The Analysis and Testing Center of HUST is also acknowledged for its analytical and testing assistance.

NOMENCLATURE

EED	electro-electrodialysis
AEMs	anion-exchange membranes
TMHDA	*N,N,N′,N′*-tetramethyl-1,6-hexanediamine
TMA	trimethylamine
DMF	*N,N*-dimethylformamide
DI	deionized
CMPSU	chloromethylated polysulfone
CQAPSU-*x*-*y*	cross-linked quaternized ammonium polysulfone with different molar ratios of quaternization reagents to CMPSU
ATR-FTIR	attenuated total reflectance-Fourier transform infrared spectroscopy
TGA	thermal gravity analysis
XPS	X-ray photoelectron spectroscopy
SEM	scanning electron microscopy
TEM	transmission electron microscopy
SAXS	small-angle X-ray scattering
NaOH	sodium hydroxide
$AgNO_3$	silver nitrate
NaCl	sodium chloride
KCl	potassium chloride
Na_2SO_4	sodium sulfate
H_3PO_4	phosphoric acid
DCM	degree of chloromethylation
CD	cross-linking degree (%)
IEC	ion-exchange capacity (mmol/g)
WU	water uptake (%)
λ	hydration number
SR	swelling ratio (%)
R_m	membrane area resistance (Ω cm^2)
θ	scattering angle
t^-	transport number
TS	tensile strength (MPa)
η	current efficiency (%)
E	energy consumption (kWh/kg)
SR_p	swelling ratio of the AEM in the plane direction (%)
SR_t	swelling ratio of the AEM in the thick direction (%)
A_{xQA}	fitting peak area of cross-linked quaternary ammonium groups
A_{TA}	fitting peak area of tertiary amine groups
A_{QA}	fitting peak area of non-cross-linking quaternary ammonium groups
M_c	molar mass of the cation active groups (g/mol)
R_{m1}	resistance of the entire cell with a membrane (Ω cm^2)
R_{m2}	resistance of the entire cell without a membrane (Ω cm^2)
E_1	potential difference between the electrodes (V)
E_0	potential of the standard solution (V)
$C_{H_3PO_4}$	concentration of phosphoric acid solution (mol/L)
C_{AgNO_3}	concentration of $AgNO_3$ solution consumed (mol/L)
V_{AgNO_3}	volume of $AgNO_3$ solution consumed (L)
C_1	concentration of KCl solution on one side (mol/L)
C_2	concentration of KCl solution on the other side (mol/L)
W_{wet}	weight of the wet membrane (g)
L_{length}	length of the wet membrane (m)
L_{width}	width of the wet membrane (m)
L_{thick}	thickness of the wet membrane (m)
W_{dry}	weight of the dry membrane (g)
L'_{length}	length of the dry membrane (m)

https://doi.org/10.1021/acsomega.1c03720
ACS Omega 2021, 6, 32417−32430

L'_{width}	width of the dry membrane (m)
L'_{thick}	thickness of the dry membrane (m)
C	concentration of phosphoric acid solution in the anode compartment at time t (mol/L)
V	volume of phosphoric acid solution in the anode compartment at time t (L)
C_0	concentration of phosphoric acid solution in the anode compartment at time 0 (mol/L)
V_0	the volume of phosphoric acid solution in anode compartment at time 0 (L)
U	voltage drop across the membrane in EED (V)
I	current across the membrane in EED (A)
t	time during the EED test (h)
F	Faraday constant (C/mol)
T	temperature (K)
C_{mi}^{c}	initial concentration of metal ions in the cathode compartment (mol/L)
C_{mi}^{a}	intial concentration of metal ions in the anode compartment (mol/L)
C_{mf}^{a}	final concentration of metal ions in the anode compartment (mol/L)
R_e	removal rates of the metal ions (%)

REFERENCES

(1) Zhuang, H.; Zhong, Y.; Yang, L. Adsorption equilibrium and kinetics studies of divalent manganese from phosphoric acid solution by using cationic exchange resin. *Chin. J. Chem. Eng.* **2020**, *28*, 2758−2770.

(2) Wu, S.; Liangshi, W.; Patrick, Z.; Hassan, E.-S.; Brij, M.; Xiaowei, H.; Longsheng, Z.; Lifeng, Z.; Zongyu, F. Simultaneous recovery of rare earths and uranium from wet process phosphoric acid using solvent extraction with D2EHPA. *Hydrometallurgy* **2018**, *175*, 109−116.

(3) Abdel-Ghafar, H. M.; et al. Purifiation of high iron wet-process phosphoric acid via oxalate precipitation method. *Hydrometallurgy* **2019**, *184*, 1−8.

(4) Touaibia, D.; Kerdjoudj, H.; et al. Concentration and purification of wet industrial phosphoric acid by electro-electro-dialysis. *J. Appl. Electrochem.* **1996**, *26*, 1071−1073.

(5) Zhuang, H.; Yanjun, Z.; Lin, Y. Adsorption equilibrium and kinetics studies of divalent manganese from phosphoric acid solution by using cationic exchange resin. *Chin. J. Chem. Eng.* **2020**, *28*, 2758−2770.

(6) Ottosen, L. M.; Jensen, P. E.; Kirkelund, G. M. Electrodialytic separation of phosphorus and heavy metals from two types of sewage sludge ash. *Sep. Sci. Technol.* **2014**, *49*, 1910−1920.

(7) Cheira, M. F.; Rashed, M.; Mohamed, A.; Hussein, G.; Awadallah, M. Removal of some harmful metal ions from wet-process phosphoric acid using murexide-reinforced activated bentonite. *Mater. Today Chem.* **2019**, *14*, No. 100176.

(8) Iravaninia, M.; Azizi, S.; Rowshanzamir, S. A comprehensive study on the stability and ion transport in cross-linked anion exchange membranes based on polysulfone for solid alkaline fuel cells. *Int. J. Hydrogen Energy* **2017**, *42*, 17229−17241.

(9) Hossain, M. M.; Wu, L.; Liang, X.; Yang, Z.; Hou, J.; Xu, T. Anion exchange membrane crosslinked in the easiest way stands out for fuel cells. *J. Power Sources* **2018**, *390*, 234−241.

(10) Duan, X.; Wang, C.; Wang, T.; Xie, X.; Zhou, X.; Ye, Y. A polysulfone-based anion exchange membrane for phosphoric acid concentration and purification by electro-electrodialysis. *J. Membr. Sci.* **2018**, *552*, 86−94.

(11) Sata, T. *Ion Exchange Membranes: Preparation, Characterization, Modification and Application*; Royal Society of Chemistry: Cambridge, 2007.

(12) Han, B.; Pan, J.; Yang, S.; Zhou, M.; Li, J.; Sotto Diaz, A.; Van der Bruggen, B.; Gao, C.; Shen, J. Novel composite anion exchange membranes based on quaternized polyepichlorohydrin for electro-membrane application. *Ind. Eng. Chem. Res.* **2016**, *55*, 7171−7178.

(13) Liu, L.; Chu, X.; Liao, J.; Huang, Y.; Li, Y.; Ge, Z.; Hickner, M. A.; Li, N. Tuning the properties of poly(2,6-dimethyl-1,4-phenylene oxide) anion exchange membranes and their performance in H_2/O_2 fuel cells. *Energy Environ. Sci.* **2018**, *11*, 435−446.

(14) Yang, C.; Liu, L.; Han, X.; Huang, Z.; Dong, J.; Li, N. Highly anion conductive, alkyl-chain-grafted copolymers as anion exchange membranes for operable alkaline H_2/O_2 fuel cells. *J. Mater. Chem. A* **2017**, *5*, 10301−10310.

(15) Duan, X.; Wang, C.; Wang, T.; Xie, X.; Zhou, X.; Ye, Y. Comb-shaped anion exchange membrane to enhance phosphoric acid purification by electro-electrodialysis. *J. Membr. Sci.* **2019**, *573*, 64−72.

(16) Bai, T.; Wang, M.; Zhang, B.; Jia, Y.; Chen, Y. Anion-exchange membrane with ion-nanochannels to beat trade-off between membrane conductivity and acid blocking performance for waste acid reclamation. *J. Membr. Sci.* **2019**, *573*, 657−667.

(17) Kim, K.; Jung, B.-K.; Ko, T.; Kim, T.-H.; Lee, J.-C. Comb-shaped polysulfones containing sulfonated polytriazole side chains for proton exchange membranes. *J. Membr. Sci.* **2018**, *554*, 232−243.

(18) Mondal, A. N.; He, Y.; Wu, L.; Khan, M. I.; Emmanuel, K.; Hossain, M. M.; Ge, L.; Xu, T. Click mediated high-performance anion exchange membranes with improved water uptake. *J. Mater. Chem. A* **2017**, *5*, 1022−1027.

(19) Guo, M.; Zhang, M.; He, D.; Hu, J.; Wang, X.; Gong, C.; Xie, X.; Xue, Z. Comb-like solid polymer electrolyte based on polyethylene glycol-grafted sulfonated polyether ether ketone. *Electrochim. Acta* **2017**, *255*, 396−404.

(20) Zhu, L.; Pan, J.; Wang, Y.; Han, J.; Zhuang, L.; Hickner, M. A. Multication side chain anion exchange membranes. *Macromolecules* **2016**, *49*, 815−824.

(21) Xu, Y.; Ye, N.; Zhang, D.; Yang, J.; He, R. Ionic crosslinking of imidazolium functionalized poly(aryl ether ketone) by sulfonated poly(ether ether ketone) for anion exchange membranes. *J. Colloid Interface Sci* **2017**, *497*, 333−342.

(22) Hou, J.; Liu, Y.; Ge, Q.; Yang, Z.; Wu, L.; Xu, T. Recyclable cross-linked anion exchange membrane for alkaline fuel cell application. *J. Power Sources* **2018**, *375*, 404−411.

(23) Hu, J.; Wang, W.; Zhou, B.; Feng, Y.; Xie, X.; Xue, Z. Poly(ethylene oxide)-based composite polymer electrolytes embedding with ionic bond modified nanoparticles for all-solid-state lithium-ion battery. *J. Membr. Sci.* **2019**, *575*, 200−208.

(24) Tibbits, A. C.; Mumper, L. E.; Kloxin, C. J.; Yan, Y. S. A Single-Step Monomeric Photo-Polymerization and Crosslinking via Thiol-Ene Reaction for Hydroxide Exchange Membrane Fabrication. *J. Electrochem. Soc.* **2015**, *162*, F1206−F1211.

(25) Kwon, S.; Rao, A. H. N.; Kim, T.-H. Anion exchange membranes based on terminally crosslinked methyl morpholinium-functionalized poly(arylene ether sulfone)s. *J. Power Sources* **2018**, *375*, 421−432.

(26) Xue, J.; Liu, L.; Liao, J.; Shen, Y.; Li, N. UV-crosslinking of polystyrene anion exchange membranes by azidated macromolecular crosslinker for alkaline fuel cells. *J. Membr. Sci.* **2017**, *535*, 322−330.

(27) Sheng, F.; Hou, L.; Wang, X.; Irfan, M.; Shehzad, M. A.; Wu, B.; Ren, X.; Ge, L.; Xu, T. Electro-nanofiltration membranes with positively charged polyamide layer for cations separation. *J. Membr. Sci.* **2020**, *594*, No. 117453.

(28) Du, X.; Wang, Z.; Liu, W.; Xu, J.; Chen, Z.; Wang, C. Imidazolium-functionalized poly (arylene ether ketone) cross-linked anion exchange membranes. *J. Membr. Sci.* **2018**, *566*, 205−212.

(29) Pan, Q.; Hossain, M. M.; Yang, Z.; Wang, Y.; Wu, L.; Xu, T. One-pot solvent-free synthesis of cross-linked anion exchange membranes for electrodialysis. *J. Membr. Sci.* **2016**, *515*, 115−124.

(30) He, Y.; Wu, L.; Pan, J.; Zhu, Y.; Ge, X.; Yang, Z.; Ran, J.; Xu, T. A mechanically robust anion exchange membrane with high hydroxide conductivity. *J. Membr. Sci.* **2016**, *504*, 47−54.

(31) Hao, J.; Jiang, Y.; Gao, X.; Lu, W.; Xiao, Y.; Shao, Z.; Yi, B. Functionalization of polybenzimidazole-crosslinked poly (vinylbenzyl

https://doi.org/10.1021/acsomega.1c03720
ACS Omega 2021, 6, 32417−32430

chloride) with two cyclic quaternary ammonium cations for anion exchange membranes. *J. Membr. Sci.* **2018**, *548*, 1−10.
(32) Jeevanantham, S.; Hosimin, S.; Vengatesan, S.; Sozhan, G. Quaternized poly(styrene-co-vinylbenzyl chloride) anion exchange membranes: role of different ammonium cations on structural, morphological, thermal and physio-chemical properties. *New J. Chem.* **2018**, *42*, 380−387.
(33) Hao, J.; Gao, X.; Jiang, Y.; Zhang, H.; Luo, J.; Shao, Z.; Yi, B. Crosslinked high-performance anion exchange membranes based on poly(styrene-b-(ethylene-co-butylene)-b-styrene. *J. Membr. Sci.* **2018**, *551*, 66−75.
(34) Chen, N.; Long, C.; Li, Y.; Wang, D.; Zhu, H. High-performance layered double hydroxide/poly(2,6-dimethyl-1,4-phenylene oxide) membrane with porous sandwich structure for anion exchange membrane fuel cell applications. *J. Membr. Sci.* **2018**, *552*, 51−60.
(35) Yu, S.; Ma, X.; Liu, H.; Hao, J. Highly stable double crosslinked membrane based on poly (vinylbenzyl chloride) for anion exchange membrane fuel cell. *Polym. Bull.* **2018**, *75*, 5163−5177.
(36) Mo, Z.-H.; Yang, R.; Hong, S.; Wu, Y.-X. In-situ preparation of cross-linked hybrid anion exchange membrane of quaternized poly (styrene-b-isobutylene-b-styrene) covalently bonded with graphene. *Int. J. Hydrogen Energy* **2018**, *43*, 1790−1804.
(37) Yang, S.; Kim, W.-S.; Choi, J.; Choi, Y.-W.; Jeong, N.; Kim, H.; Nam, J.-Y.; Jeong, H.; Kim, Y. H. Fabrication of photocured anion-exchange membranes using water-soluble siloxane resins as cross-linking agents and their application in reverse electrodialysis. *J. Membr. Sci.* **2019**, *573*, 544−553.
(38) Dai, P.; Mo, Z.; Xu, R.; Zhang, S.; Wu, Y. Cross-linked quaternized poly(styrene-b-(ethylene-co-butylene)-b-styrene) for anion exchange membrane: synthesis, characterization and properties. *ACS Appl. Mater. Interfaces* **2016**, *8*, 20329−20341.
(39) Xu, M.; Gang, M.; Cao, L.; He, X.; Song, Y.; Jiang, Z.; Wu, H.; Su, Y. Enhanced hydroxide ion conductivity of imidazolium functionalized poly (ether ether ketone) membrane by incorporating N,N,N′,N′-tetramethyl-1,4-phenylenediamine. *Solid State Ionics* **2018**, *325*, 163−169.
(40) Zhou, J.; Chen, P.; Shi, Q.; Wang, R.; Chen, X.; An, Z. Cross-linked poly (arylene ether sulfone) s with side-chain aromatic benzyltrimethyl ammonium for anion-exchange membranes. *Polym. Bull.* **2017**, *74*, 4329−4348.
(41) Lin, X.; Kim, S.; Zhu, D. M.; Shamsaei, E.; Xu, T.; Fang, X.; Wang, H. Preparation of porous diffusion dialysis membranes by functionalization of polysulfone for acid recovery. *J. Membr. Sci.* **2017**, *524*, 557−564.
(42) Mohanty, A. D.; Ryu, C. Y.; Kim, Y. S.; Bae, C. Stable elastomeric anion exchange membranes based on quaternary ammonium-tethered polystyrene-b-poly(ethylene-co-butylene)-b-polystyrene triblock copolymers. *Macromolecules* **2015**, *48*, 7085−7095.
(43) Zeng, Q.; Liu, Q.; Broadwell, I.; Zhu, A.; Xiong, Y.; Tu, X. Anion exchange membranes based on quaternized polystyrene-block-poly(ethylene-ran-butylene)-block-polystyrene for direct methanol alkaline fuel cells. *J. Membr. Sci.* **2010**, *349*, 237−243.
(44) Li, Z.; He, X.; Jiang, Z.; Yin, Y.; Zhang, B.; He, G.; Tong, Z.; Wu, H.; Jiao, K. Enhancing hydroxide conductivity and stability of anion exchange membrane by blending quaternary ammonium functionalized polymers. *Electrochim. Acta* **2017**, *240*, 486−494.
(45) Yu, S.; Zhu, J.; Liao, J.; Ruan, H.; Sotto, A.; Shen, J. Homogeneous trimethylamine-quaternized polysulfone-based anion exchange membranes with crosslinked structure for electrodialysis desalination. *Sep. Purif. Technol.* **2021**, *257*, No. 117874.
(46) Xie, F.; Gao, X.; Hao, J.; Yu, H.; Shao, Z.; Yi, B. Preparation and properties of amorphous TiO2 modified anion exchange membrane by impregnation-hydrolysis method. *React. Funct. Polym.* **2019**, *144*, No. 104348.
(47) Zhang, X.; Fan, C.; Yao, N.; Zhang, P.; Hong, T.; Xu, C.; Cheng, J. Quaternary $Ti_3C_2T_x$ enhanced ionic conduction in quaternized polysulfone membrane for alkaline anion exchange membrane fuel cells. *J. Membr. Sci.* **2018**, *563*, 882−887.
(48) Han, J.; Liu, Q.; Li, X.; Pan, J.; Wei, L.; Wu, Y.; Peng, H.; Wang, Y.; Li, G.; Chen, C. An effective approach for alleviating cation-induced backbone degradation in aromatic ether-based alkaline polymer electrolytes. *ACS Appl. Mater. Interfaces* **2015**, *7*, 2809−2816.
(49) Le Mong, A.; Kim, D. Alkaline anion exchange membrane from poly(arylene ether ketone)-g-polyimidazolium copolymer for enhanced hydroxide ion conductivity and thermal, mechanical, and hydrolytic stability. *Electrochim. Acta* **2018**, *290*, 544−555.
(50) Chen, W.; Yan, X.; Wu, X.; Huang, S.; Luo, Y.; Gong, X.; He, G. Tri-quaternized poly (ether sulfone) anion exchange membranes with improved hydroxide conductivity. *J. Membr. Sci.* **2016**, *514*, 613−621.
(51) He, Y.; Pan, J.; Wu, L.; Zhu, Y.; Ge, X.; Ran, J.; Yang, Z.; Xu, T. A novel methodology to synthesize highly conductive anion exchange membranes. *Sci. Rep.* **2015**, *5*, No. 13417.
(52) Krathumkhet, N.; Vongjitpimol, K.; Chuesutham, T.; Changkhamchom, S.; Phasuksom, K.; Sirivat, A.; Wattanakul, K. Preparation of sulfonated zeolite ZSM-5/sulfonated polysulfone composite membranes as PEM for direct methanol fuel cell application. *Solid State Ionics* **2018**, *319*, 278−284.
(53) Tanaka, Y. *Ion Exchange Membranes: Fundamentals and Applications*; Elsevier: Amsterdam, 2007.
(54) Dai, P.; Mo, Z.; Xu, R.; Zhang, S.; Lin, X.; Lin, W.; Wu, Y. Development of a cross-linked quaternized poly(styrene-b-isobutylene-b-styrene)/graphene oxide composite anion exchange membrane for direct alkaline methanol fuel cell application. *RSC Adv.* **2016**, *6*, 52122−52130.
(55) Wang, W.; Wang, S.; Li, W.; Xie, X.; lv, Y. Synthesis and characterization of a fluorinated cross-linked anion exchange membrane. *Int. J. Hydrogen Energy* **2013**, *38*, 11045−11052.
(56) Ul Afsar, N.; Ge, X.; Zhao, Z.; Hussain, A.; He, Y.; Ge, L.; Xu, T. Zwitterion membranes for selective cation separation via electrodialysis. *Sep. Purif. Technol.* **2021**, *254*, No. 117619.
(57) Li, F.-r.; Jia, Y.-x.; Guo, R.-q.; Wang, M. Preparation of composite anion-exchange membrane with acid-blocking performance for brine reclamation by bipolar membrane electrodialysis. *Sep. Purif. Technol.* **2021**, *254*, No. 117587.
(58) Ran, J.; Wu, L.; He, Y.; Yang, Z.; Wang, Y.; Jiang, C.; Ge, L.; Bakangura, E.; Xu, T. Ion exchange membranes: new developments and applications. *J. Membr. Sci.* **2017**, *522*, 267−291.
(59) Khan, M. I.; Mondal, A. N.; Tong, B.; Jiang, C.; Emmanuel, K.; Yang, Z.; Wu, L.; Xu, T. Development of BPPO-based anion exchange membranes for electrodialysis desalination applications. *Desalination* **2016**, *391*, 61−68.
(60) Khan, M. I.; Zheng, C.; Mondal, A. N.; Hossain, M. M.; Wu, B.; Emmanuel, K.; Wu, L.; Xu, T. Preparation of anion exchange membranes from BPPO and dimethylethanolamine for electrodialysis. *Desalination* **2017**, *402*, 10−18.
(61) Wei, X.; Wang, Y.; Yan, H.; Jiang, C.; Xu, T. A sustainable valorization of neopentyl glycol salt waste containing sodium formate via bipolar membrane electrodialysis. *Sep. Purif. Technol.* **2021**, *254*, No. 117563.
(62) Fu, L.; Gao, X.; Yang, Y.; Aiyong, F.; Hao, H.; Gao, C. Preparation of succinic acid using bipolar membrane electrodialysis. *Sep. Purif. Technol.* **2014**, *127*, 212−218.
(63) Pisarska, B.; Jaroszek, H.; Mikołajczak, W.; Nowak, M.; Cichy, B.; Stopa, H.; Markowicz, P. Application of electro-electrodialysis for processing of sodium sulphate waste solutions containing organic compounds: Preliminary study. *J. Cleaner Prod.* **2017**, *142*, 3741−3747.
(64) Gao, W.; Fang, Q.; Yan, H.; Wei, X.; Wu, K. Recovery of Acid and Base from Sodium Sulfate Containing Lithium Carbonate Using Bipolar Membrane Electrodialysis. *Membranes* **2021**, *11*, 152.
(65) Jaroszek, H.; Mikołajczak, W.; Nowak, M.; Pisarska, B. Comparison of the applicability of selected anion-exchange membranes for production of sulfuric acid by electro-electrodialysis. *Desalination Water Treat.* **2017**, *64*, 223−227.

https://doi.org/10.1021/acsomega.1c03720
ACS Omega 2021, 6, 32417−32430

(66) Chen, X.; Chen, G. Q.; Wang, Q.; Xu, T.; Kentish, S. E. Transforming salty whey into cleaning chemicals using electrodialysis with bipolar membranes. *Desalination* **2020**, *492*, No. 114598.

https://doi.org/10.1021/acsomega.1c03720
ACS Omega 2021, 6, 32417−32430